END

FILMED

DTIC

||| **1·0**

2·8   2·5

3·15   2·2

3·5

4·0   2·0

4·5

1·8

||| **1·1**

||| **1·25** ||| **1·4** ||| **1·6**

NATIONAL BUREAU OF STANDARDS
MICROCOPY RESOLUTION TEST CHART

AD-A163 077

Ferrofluid Hydroacoustic Projector

Mark S. Ptak and Pieter S. Dubbelday

Underwater Sound Reference Detachment
P.O. Box 8337
Orlando, Florida 32856-8337

November 30, 1985

DTIC
ELECTE
JAN 1 3 1986

B

NAVAL RESEARCH LABORATORY
Washington, D.C. 20375-5000

86 1 13 132

REPORT DOCUMENTATION PAGE

1a REPORT SECURITY CLASSIFICATION	1b. RESTRICTIVE MARKINGS
UNCLASSIFIED	N/A *AI63 077*

2a SECURITY CLASSIFICATION AUTHORITY	3 DISTRIBUTION/AVAILABILITY OF REPORT
N/A	Approved for public release;
2b DECLASSIFICATION/DOWNGRADING SCHEDULE	distribution unlimited.
N/A	

4 PERFORMING ORGANIZATION REPORT NUMBER(S)	5 MONITORING ORGANIZATION REPORT NUMBER(S)
None	NRL Memorandum Report 5644

6a NAME OF PERFORMING ORGANIZATION	6b OFFICE SYMBOL (If applicable)	7a. NAME OF MONITORING ORGANIZATION
Florida Institute of Technology		Underwater Sound Reference Detachment Naval Research Laboratory

6c ADDRESS (City, State, and ZIP Code)	7b. ADDRESS (City, State, and ZIP Code)
P.O. Box 1150 Melbourne, FL 32901	P.O. Box 8337 Orlando, FL 32856-8337

8a. NAME OF FUNDING/SPONSORING ORGANIZATION	8b. OFFICE SYMBOL (If applicable)	9. PROCUREMENT INSTRUMENT IDENTIFICATION NUMBER
Chief of Naval Research	513	N00014-80-C-0932

8c ADDRESS (City, State, and ZIP Code)	10 SOURCE OF FUNDING NUMBERS			
800 N. Quincy Street Arlington, VA 22217	PROGRAM ELEMENT NO	PROJECT NO	TASK NO.	WORK UNIT ACCESSION NO
	61153N			59-0582-0

11 TITLE (Include Security Classification)

FERROFLUID HYDROACOUSTIC PROJECTOR

12 PERSONAL AUTHOR(S)
Mark S. Ptak and Pieter S. Dubbelday

13a TYPE OF REPORT	13b TIME COVERED	14 DATE OF REPORT (Year, Month, Day)	15 PAGE COUNT
Final	FROM 9/80 TO 12/83	November 30, 1985	52

16 SUPPLEMENTARY NOTATION

17 COSATI CODES			18. SUBJECT TERMS (Continue on reverse if necessary and identify by block number)
FIELD	GROUP	SUB-GROUP	Ferrofluid; Magnetic fluids; Projector
20	01		

19 ABSTRACT (Continue on reverse if necessary and identify by block number)

A hydroacoustic projector has been constructed with a ferrofluid as the magneto-acoustic transduction material. It has a toroidal shape; a dc magnetic bias field magnetizes the particles, and an ac field causes bulk movement of the fluid inside the toroid, as contrasted with magnetostriction. The construction of a prototype projector is described. The outer diameter of the ferrofluid cavity is 17.2 cm, its height is 8.3 cm. The inner wall is adjoined by a layer of air that functions as a pressure-release surface. The operation of the projector was measured in a wooden test tank. The pressure was measured by an NRL-USRD type F61 hydrophone, and the particle velocity by means of hot-film anemometry. As predicted by theory, the frequency of the acoustic field without bias field is predominantly double that of the exciting frequency; with bias field the single frequency appears in the acoustic measurements. The experimental results show strong resonances from 10 to 100 Hz. They are tentatively ascribed to flexural resonances in the walls of the tank. Further experiments are needed to definitely rule out   (over)

20 DISTRIBUTION/AVAILABILITY OF ABSTRACT	21 ABSTRACT SECURITY CLASSIFICATION
☒ UNCLASSIFIED/UNLIMITED ☐ SAME AS RPT ☐ DTIC USERS	UNCLASSIFIED

22a NAME OF RESPONSIBLE INDIVIDUAL	22b TELEPHONE (Include Area Code)	22c OFFICE SYMBOL
Dr. Pieter S. Dubbelday	305, 857-5197	5975

DD FORM 1473, 84 MAR

83 APR edition may be used until exhausted
All other editions are obsolete

SECURITY CLASSIFICATION OF THIS PAGE

Abstract (cont'd.)

other sources of sound not originating in the ferrofluid.

DTIC
ELECTE
JAN 1 3 1986
S   D
B

Accession For
NTIS   CRA&I   ✓
DTIC
C
Justification

By
Distribution/
Availability Codes
Dist   Avail and/or
         Special

A-1

CONTENTS

CONTENTS (cont'd.)

FERROFLUID HYDROACOUSTIC PROJECTOR

I. INTRODUCTION

A. Background

Ferromagnetic liquids are not known to exist in nature, but fluids with magnetic properties can be manufactured. The first reports of the development of such a fluid came in the early 1960's. One of the early patents for ferrofluid is held by Papell [1]. Papell's fluid is described and its behavior is analyzed in a paper by Papell and Faber [2]. Many applications for these fluids have been suggested; several of these, including rotary shaft seals and hydrodynamic bearings, have already found their way into common usage. Perry [3] gives an overview of some current ferrofluid applications. Use of ferrofluid as an acoustic transduction material has been considered by Carey and Fenlon [4], Overby [5], and Dubbelday [6]. The work presented in this report is the design, construction, testing, and analysis of an underwater sound projector based on a theoretical design given by Dubbelday [6]. A patent for this design has been obtained by Dubbelday and Timme [7]. Overby's design has also received a patent [8]. Presently the most common transducers available are of the magnetostrictive, moving-coil, or piezoelectric type. In the toroidal design described here, the bulk movement of the ferrofluid couples to the acoustic medium. It is intended for operation at low frequency. Because the ferrofluid transducer material is a liquid, there is no limitation to the static pressure that can be sustained. Moreover, there is complete freedom from damage by shock or excessive displacement stress, an important advantage over the very brittle piezoelectric and magnetostrictive materials. The device can be operated in a free-flooded condition; therefore, there is no need for cumbersome and heavy pressure-compensation materials. The specific gravity of the ferrofluid is only slightly larger than 1 (typically 1.20); therefore, buoyancy will provide the major part of the force needed to support and contain the device.

Before the design and prototype constructions are described, some background material on the ferrofluid itself will be given.

B.   Ferrofluids

Ferrofluids consist of subdomain ferromagnetic grains (usually less than
100 Å in diameter) coated with a monomolecular surfactant and suspended in a
carrier liquid. The surfactant coatings act as "bumpers" between the grains
and serve to overcome the attractive magnetic and Van der Waals forces that
otherwise would cause the grains to agglomerate and settle out of suspension.
A great deal of work has been done to determine which surfactants lead to the
greatest stability (see Ref. 9, for example). For the purposes of this work,
however, the only concerns are: (1) the overall characteristics of the
ferrofluid (such as density), which are dependent upon the choice of the
carrier liquid; and (2) the ferrofluid's magnetization characteristics. The
physical chemistry of ferrofluids will not be discussed here. Carrier liquids
for commercially available ferrofluids include hydrocarbons, fluorocarbons,
diesters, and water.

Ferrofluids react to magnetic fields through the interaction of the field
with the permanent magnetic moment of each particle. Any particle motions
that result are transmitted to the carrier liquid through viscous drag forces.
Therefore, consideration must be given to the orientation of the magnetic
moment within the body of the ferromagnetic grains. Because ferromagnetic
materials have a crystalline structure, the magnetic properties are not the
same in every direction (magnetic anisotropy). The anisotropy energy is that
energy needed to rotate the magnetic moment away from the preferred crystal
axes into a "hard" direction. If the thermal energy of the grains is much
greater than the anisotropy energy, the magnetic moments are free to move
independently of any physical grain motion. This behavior is called
superparamagnetism, due to the similarity between the theory of this behavior
and the theory governing moment-bearing atoms (see Ref. 10). If the
anisotropy energy is much greater than the thermal energy of the grains, then
the magnetic moments are locked rigidly into place within each grain. If the
thermal and anisotropy energies are comparable, the behavior is somewhere
between these two cases. Berkovsky [11] gives a more complete description of
this situation.

An external magnetic field can interact with the magnetic moment of the ferromagnetic grains in two ways. The field can result in a body force and a body couple. The couple can exist only when the magnetic moment and the magnetic field are non-collinear ($\vec{M} \times \vec{H} \neq 0$). If the magnetic moment of each particle is independent of particle orientation, then a body couple would rotate the magnetic moments but not the ferromagnetic grains themselves. If the magnetic moments are "frozen" into the particles, a body couple would physically rotate all the grains with magnetic moments not parallel to the magnetic field. Study of the dynamics of ferrofluid magnetization [12] reveals evidence of both types of behavior under normal operating conditions.

Under quasi-static conditions, body couples do not exist and effects of magnetic anisotropy become unimportant. The magnetization characteristics of ferrofluid under these conditions are adequately described by superparamagnetic theory. Application of superparamagnetic theory to ferrofluids is discussed by Kaiser and Miskolczy [13]. The result is a magnetization curve like that given in Fig. 1. Bias field H_b and modulation H_{ac} are discussed in Sec. III. B. The form of $M(H)$ is the Langevin function. The asymptotic value of M under increasing field is the saturation magnetization. The magnetic susceptibility approaches zero.

The ferrofluid used in this work is a water-based ferrofluid, called Lignosite FML, manufactured by the Georgia-Pacific Corporation. It is presently available with a saturation magnetization of 140 G, but a 240-G fluid is being developed. Lignosite FML is composed of iron lignosulfonate. The reason this fluid was chosen was its reasonable price. Ferrofluids with much higher saturation magnetizations are available from the Ferrofluidics Corporation for a considerably higher price. A magnetization curve for Lignosite FML is shown in Fig. 1. This curve was plotted from data supplied by the manufacturer.

C. Previous Work

Carey and Fenlon [4] performed a theoretical study of the possible application of ferrofluids as acoustic transducer materials in 1969. They considered two possible modes of operation: modulation of the
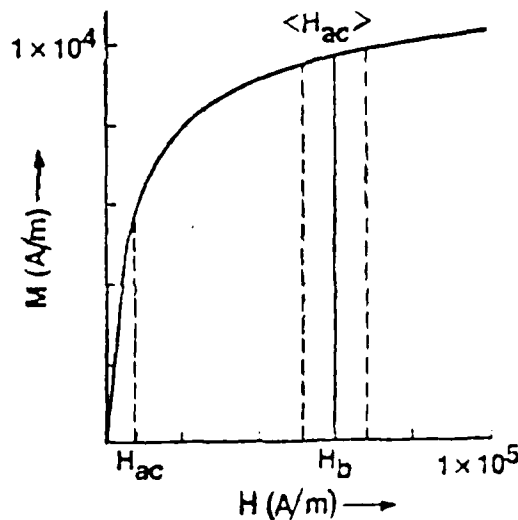
Fig. 1 - Ferrofluid magnetization curve

magnetostrictive effect experienced by a ferrofluid in a magnetic field and modulation of the bulk motion of the ferrofluid generated by a nonuniform magnetic field. The predicted performance of the ferrofluid was compared with that of conventional transducer materials, and observations were made concerning frequency ranges and conditions under which ferrofluids would have some advantages over other materials.

From the results of their calculations, Carey and Fenlon conclude that the magnetostrictive mode of operation is too inefficient to compete with conventional magnetostrictive materials. They also conclude that the bulk motion modulation of ferrofluids might be a desirable alternative to conventional means of transduction for some applications, such as use in severe environments and in situations where a wideband frequency response is required. The configuration they propose for a transducer that would operate this way is a ferrofluid-filled piston contained in a tube with one end open to the air and the other end exposed to the water. The ferrofluid piston is put into a time-varying magnetic-field gradient. The details of how this time-varying magnetic-field gradient would be generated were not discussed.

In 1978, Overby [5] built a prototype ferrofluid sound projector with a
design roughly like that of Carey and Fenlon. Ferrofluid was contained in a
cylindrical cavity with elastomer ends. The cavity was then surrounded with a
solenoidal coil that carried both ac and dc. The purpose of the dc was to
bring the ferrofluid to magnetic saturation. As will be shown in Chapter III,
a force is generated in a ferrofluid by a nonuniform magnetic field. The
expression for the force is proportional to the product of the magnetization
(M) and the magnetic-field intensity (H). If the magnetization is field
dependent, nonlinearities are introduced in the behavior. Therefore, to avoid
nonlinear behavior and to get a stronger force in the fluid, a large, static
magnetic field is generated in the fluid. In Overby's projector the ac in the
coil generated the modulating field. The design used by Overby was not
efficient because the field gradients needed to generate bulk motion of the
ferrofluid were present only near the cylinder ends. The fields in the space
occupied by most of the ferrofluid were spatially uniform and exerted no force
on the ferrofluid. The results of Overby's experiment were inconclusive.

Polunin [14,15] has proposed ferrofluid transducers with both cylindrical
and plane geometries. These transducers were designed for use at ultrasonic
frequencies.

Dubbelday [6] proposed a more efficient piston-type projector in 1980.
The alternating current was run in two coils to establish a magnetic field
gradient between the ends of a ferrofluid-filled piston. A bias field was
also a feature of this design. While no prototype was built to test this
design, the calculations showed that it would be competitive with conventional
transducers. In the same paper, the toroidal design was proposed; a later
article [16] reports on the construction of and measurements on a toroidal
projector. Ferrofluid is enclosed in a toroidal cavity with rigid top and
bottom and elastomer sidewalls (see Figs. 2 & 3). Coils carrying both ac and
dc are used to generate a modulated force in the radial direction. The radial
force causes oscillation of the ferrofluid between the elastomer walls. The
inner elastomer wall is provided with a pressure-release backing. The outer
wall is exposed to the surrounding water. The pressure-release backing
ensures that the projector will operate as a monopole radiator. The details
of this design and the construction and analysis of a prototype projector are

the subject of this report. One can show that for a given number of ampere-turns the maximum ac driving force is obtained if the current carriers do not penetrate the ferrofluid cavity. When the toroid is of relatively small size and the inner hole is not large enough to accommodate the current carriers, it might be advantageous to let the current run through the ferrofluid chamber. The wiring scheme in Fig. 3 constitutes a correction to the one given in Ref. 6.
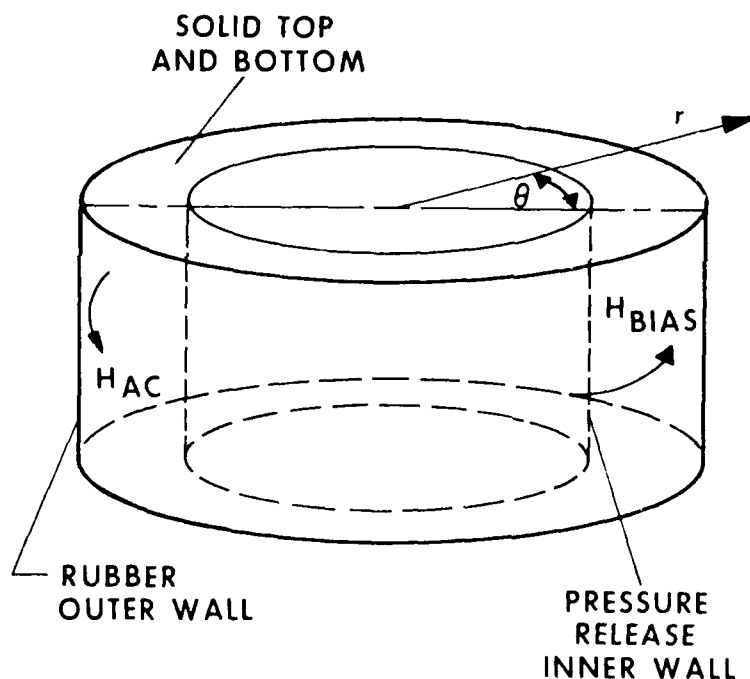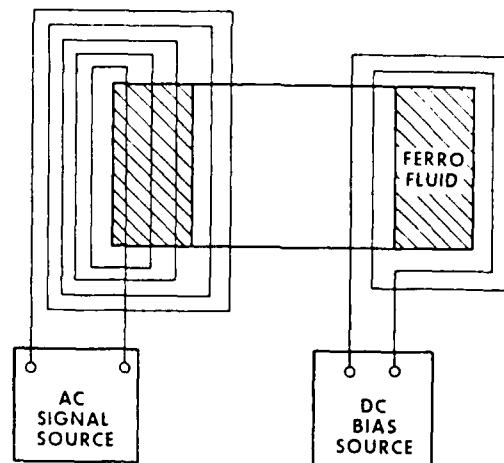

Fig. 2 - Toroidal geometry

Fig. 3 - Field generating coils in toroidal design

II. PROTOTYPE DESIGN AND CONSTRUCTION

A. Introduction

The analysis presented in Chapter III shows that for a toroidal configuration, magnetic fields in the azimuthal direction result in body forces in the ferrofluid in the radial direction. The design and construction of a prototype transducer are detailed in this chapter. The Appendix provides a list of all the materials used in the prototype.

B. Ferrofluid Core

Central to the design is a cavity to contain the ferrofluid while allowing its oscillations to be coupled to the surrounding water. The dimensions and materials used in the prototype core are shown in Figs. 4 and 5. The core was made in two halves so that the field-generating coils could
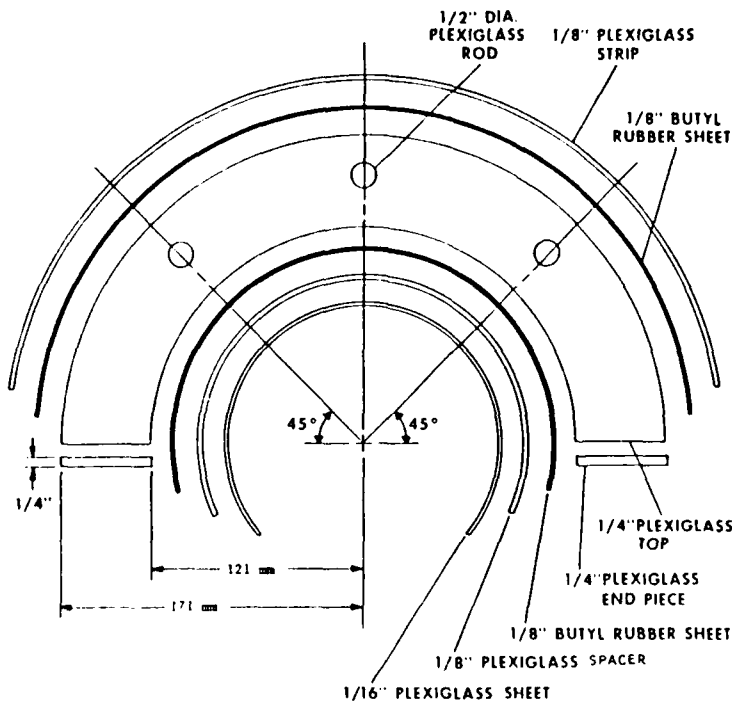
Material dimensions are in inch/
pound system to correspond with
manufacturer's sizing.
Metric conversions are:

Inch	mm
1/16	1.59
1/8	3.18
1/4	6.35
1/2	12.7

Fig. 4 - Layout of 1/2-toroid construction

be slipped over each half before they were joined. The choice of the
dimensions used in the prototype was dictated by considerations to be outlined
in Section C of this chapter. Each half of the toroidal core had to be filled
and sealed independently. The top, bottom, and ends of each half were made
from a 1/4-in.-thick sheet of Plexiglas. (Plexiglas is a tradename for
polymethyl methacrylate.) The tops and bottoms of each half were held in
place by three 1/2-in.-diam. Plexiglas rods. Pieces of 1/8-in.-thick butyl
rubber were attached at the inner and outer radii of the Plexiglas tops and
bottoms and sealed along the edges to make an airtight cavity. On the outside
radius, the butyl rubber was sealed and clamped to the Plexiglas core with
epoxy and thin curved strips of Plexiglas that were secured to the core with
#4 machine screws, as shown in Fig. 5. The rubber wall at the inner radius
was provided with a pressure-release surface to ensure more efficient
radiation (monopole). The pressure release was accomplished with a layer of
air trapped between the inner rubber wall and a thin Plexiglas wall. Curved

pieces of Plexiglas were used to hold the inner rubber wall and the Plexiglas
walls apart at the edges.

Epoxy provided an airtight seal around the edges while #4 machine screws held
the assembly together. The result was a 1/8-in.-thick airspace trapped
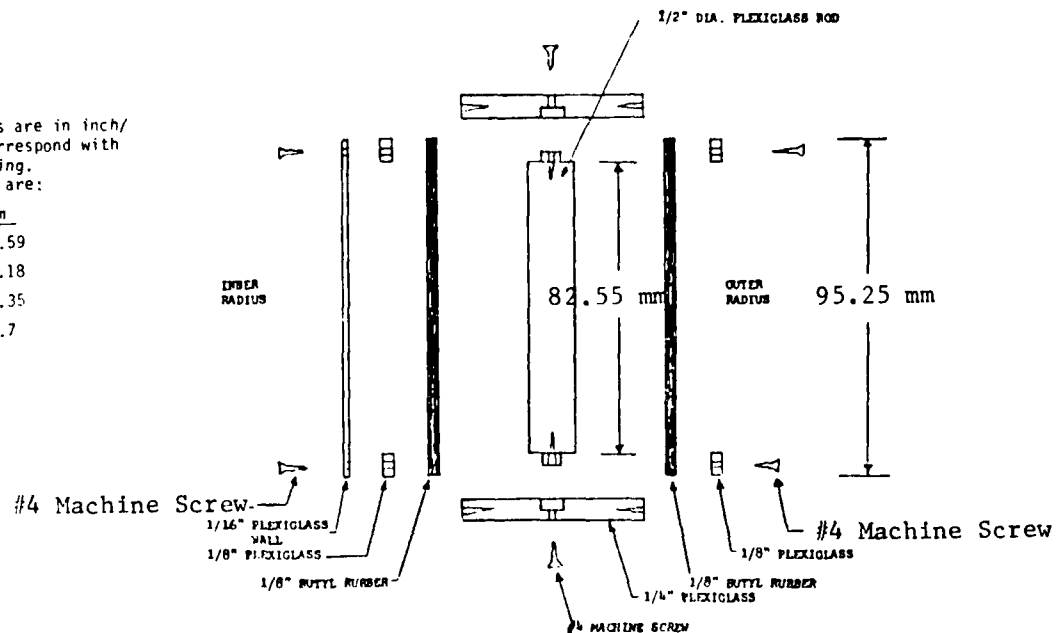against the inner wall.

Fig. 5 - Exploded side view of ferrofluid core

Depth compensation for this airspace also had to be provided. As the
transducer is submerged, hydrostatic pressure would compress the air. When
the air is compressed to the point that the inner rubber wall contacts the
thin Plexiglas wall, the ferrofluid oscillations are damped, thus rendering
the transducer useless. To prevent this from happening, a reserve airbag is
connected with the pressure-release cavity through a small plastic tube. The
reserve airbag was mounted just below the transducer.

Filling the toroid core was accomplished through holes made in the ends
of each half, as shown in Fig. 6. A gravity feed was used to fill each half
with ferrofluid. The core was filled slowly in order to minimize the number
of bubbles in the ferrofluid that might interfere with the acoustic radiation.
Seal screws were used to block the holes once the core was filled.

Ferrofluid

Hole open to air
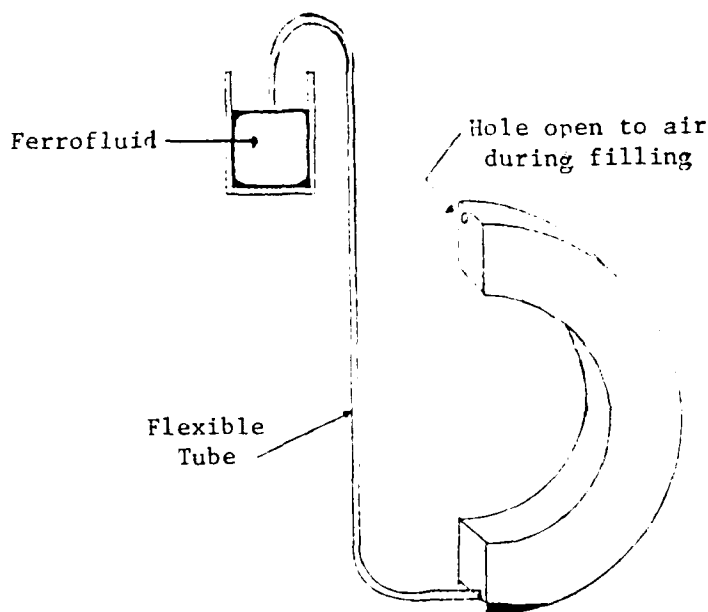during filling

Flexible
Tube

Fig. 6 - Gravity feed filling of toroid core

C. Biasing Coils

As mentioned in Chapter I, a large magnetic bias field is required to
bring the ferrofluid to magnetic saturation in order to ensure linear
operation. From Ampere's Law, the magnetic field in a toroidal coil is given
by $H = NI/2\pi R$ where N = number of turns of coil, I = current in coil, R =
radius of toroid, and H = magnetic field intensity.

The low-voltage, high-current approach for creating the magnetic bias
field was chosen for several reasons. The use of low voltages would eliminate
the need for elaborate electrical insulation for the coils. The large number
of turns in a high-voltage coil would cause more blockage of the transducer's
radiating surface and would result in heat dissipation problems. The design
illustrated in Figs. 7 and 8 was chosen to overcome these problems. Copper
plates were cut into an equal number of the C and I shapes shown in Fig. 7.
The C's and I's were joined as shown in Fig. 8. The arrows on the pieces
shown in Fig. 8 show the direction of current flow in each piece after the
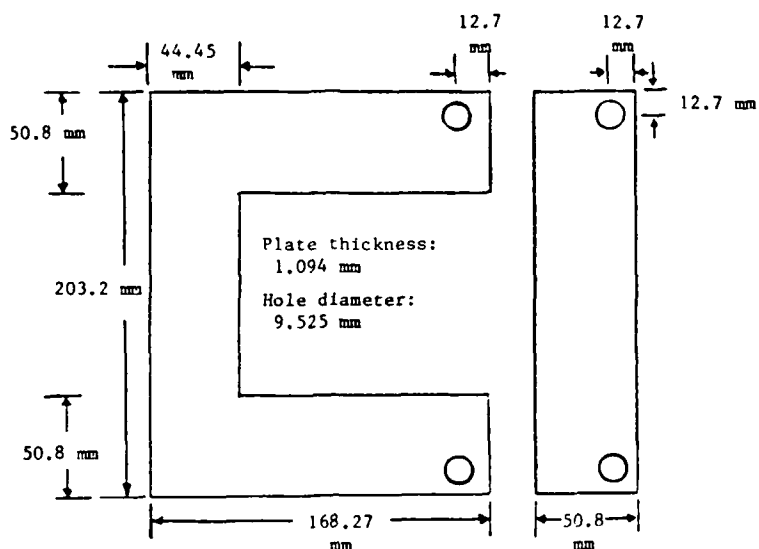coil is assembled. The resulting coil was slipped over the ferrofluid core.

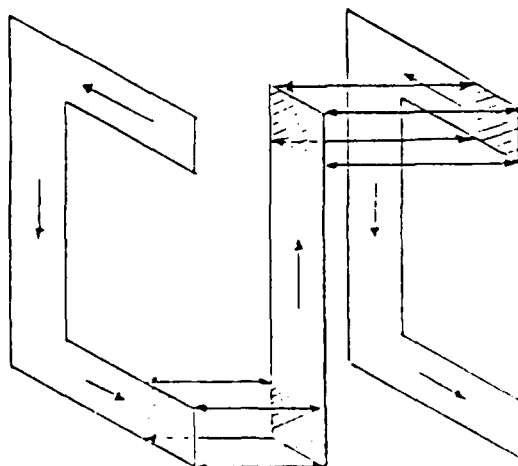Fig. 7 - Bias coil pieces before assembly

Fig. 8 - Assembly of bias coil

The turns of the coil at the outer radius were sufficiently far apart to allow for heat dissipation by free convection of the ambient water. This spacing also minimized the blockage of the radiating surface of the toroid. The dimensions shown in Fig. 7 were the result of tradeoffs among the various factors discussed above as well as the size, weight, and expense of the copper involved. The bias coil was made in two halves: one for each half of the toroid core. Each half of the bias coil had 75 turns.

The problems involved in insulating the coils were more difficult to solve than expected. The coils were first dipped in Glyptal Red Enamel (General Electric #1201), which is commonly used magnet coil paint. The coil surface was not prepared properly, and this paint scraped off rather easily--a fact that resulted in many electrical shorts in the coil after the transducer was assembled. The coils were then coated with an epoxy (West System Epoxy, Gougeon Bros., Inc.). This coating provided sufficient insulation for the purposes of this study but would not be durable enough for long-term use.

After the coil had been put on the toroidal core, the holes shown in Fig. 7 were threaded with a 1/4-in.-diam. Delrin rod. Washers formed from thin slices of 7/8-in.-diam. polyvinyl chloride (PVC) pipe were used to ensure that the coil remained properly spaced at the outer radius.

D. Modulating Coils

Two possible approaches to modulation field generation were considered for the prototype. One could attempt to modulate the large bias current in the bias coil by the use of a suitable transformer in the bias current circuit, or one could use a separate coil for the modulation field generation and tolerate the inductive coupling between the two coils. The difficulty involved in acquiring a transformer for the first approach led to the choice of the second approach for development of the prototype.

For the modulation coil, eight strands of 19 AWG magnet wire were formed into a flat coil and fixed together with Epoxy Ribbon. The resistance of this coil was 8 Ω at 70°C. This coil was made to have the same inner hole dimensions as the bias coil so that the two coils could both be slipped over

the ferrofluid core. The bias and modulation coils were merged before they
were put on the core so that the turns of the two coils alternated. The wires
in the modulation coil were formed into a flat shape for the same advantages
of heat dissipation and minimal radiation blockage that dictated the design of
the bias coil.

The modulation coils were also built in two halves. Sea Con 8-pin under-
water connectors were used to connect the two halves of the modulation coil.

E. Assembly

An aluminum stand was built to support the core and coils when they were
lifted. The stand was designed so that it would provide support for the coils
while not impeding convective water cooling of the coils during operation.
The two halves of the toroid core were each bolted to a 1/4-in.-thick sheet of
Plexiglas. The two Plexiglas sheets were finally bolted together to join the
toroid halves. The Plexiglas sheets were then bolted to the stand to hold the
entire transducer together. A 1/8-in.-thick butyl-rubber pad between the
stand and the bias coil prevented electrical contact. The aluminum stand was
coated with the same epoxy used to coat the bias coil. This coating was meant
to help prevent electrolytic action in the water surrounding the transducer.
The presence of two dissimilar metals (copper in the coils, aluminum in the
stand) in impure water will result in an electrochemical potential between the
metals with deposition of the impurities on the metal surfaces. Since bare
spots on the copper bias coils were unavoidable, it was felt that coating the
stand would help minimize electrochemical action. Moreover, it would reduce
the stray ac currents in the water that would adversely affect the operation
of the pressure transducer.

In order to test the operation of the toroidal projector, a wooden tank
was built and lined with plastic. The tank's inner dimensions are 38x31 in.,
and it was filled to a depth of approximately 1 ft. The tank was initially
filled with tap water, but once the problems were discovered with
electrochemical action, the tap water was replaced with distilled water.

III. ANALYTICAL INVESTIGATION

A. Ferrofluid Equation of Motion

Ferrofluids are a complex multiphase material. To describe the behavior
of the ferrofluid for a possible application, a model is needed that explains
the major features of this behavior but is still simple enough to handle
mathematically. A model that is suitable for the purposes of this work is one
proposed by Neuringer and Rosensweig [17] in 1964. This model assumes the
ferrofluid is a monophase, Newtonian, isotropic, nonconducting, and
incompressible continuum. The equation of motion of the ferrofluid is taken
as

$$\rho \frac{d\vec{v}}{dt} = -\nabla p + \mu \nabla^2 \vec{v} + \mu_o (\vec{M} \cdot \nabla)\vec{H} + \rho \vec{g} \tag{1}$$

where ρ = density of ferrofluid,

v = velocity,

p = pressure,

μ = dynamic viscosity,

μ_o = permeability of free space,

$\vec{M}$ = magnetization of ferrofluid,

$\vec{H}$ = magnetic field, and

$\vec{g}$ = acceleration of gravity.

This equation is the Navier-Stokes equation with an added magnetic force
term. There is some dispute over this magnetic force term; other formulations
of the force have been shown to be equally valid within the framework of the
model.   Jones [18] discusses this controversy and resolves the differences
among the various formulations of the magnetic force by showing them to be
equivalent. A more thorough discussion of the problems involved in
formulating the forces of electromagnetic fields on continuous materials is
given by Penfield and Haus [19]. Equation (2) can be simplified by omitting
the viscosity term. The relative importance of the viscosity term can be
found by calculating the Stokes number. The Stokes number is a dimensionless

number that compares viscosity and local acceleration. If the Stokes number
is much less than 1, the viscous force is relatively unimportant to the fluid
motion. The Stokes number can be written

$$St = \frac{\mu}{\rho \omega L^2} \qquad (2)$$

where L is a characteristic length of the cavity and ω is the angular
frequency of the acoustic field. Taking L = 5 cm, μ = 29 centipoise, ρ = 1230
kg/m^3, and a frequency of 100 Hz yields St = 1.5×10^{-4}. The equation of motion
of the ferrofluid is then (ignoring viscosity)

$$\rho \frac{d\vec{v}}{dt} = - \nabla p + \mu_o (\vec{M}\cdot\nabla)\vec{H} + \rho\vec{g} \ . \qquad (3)$$

The force term $(\vec{M}\cdot\nabla)\vec{H}$ must be used with care in curvilinear coordinates,
due to the fact that the directions of the coordinate axes are not constant.
For arbitrary vectors A and B in general, orthogonal coordinates ξ_1, ξ_2, and
ξ_3, the components of $(\vec{B}\cdot\nabla)\vec{A}$ along ξ_1, are given by

$$[(\vec{B}\cdot\nabla)\vec{A}]_1 = \frac{B_1}{h_1}\frac{\partial A_1}{\partial\xi_1} + \frac{B_2}{h_2}\frac{\partial A_1}{\partial\xi_2} + \frac{B_3}{h_3}\frac{\partial A_1}{\partial\xi_3}$$

$$+ \frac{A_2}{h_1 h_2}\left[B_1\frac{\partial h_1}{\partial\xi_2} - B_2\frac{\partial h_2}{\partial\xi_1}\right] + \frac{A_3}{h_1 h_3}\left[B_1\frac{\partial h_1}{\partial\xi_3} - B_3\frac{\partial h_3}{\partial\xi_1}\right] , \qquad (4)$$

where h_1, h_2, and h_3 are the scale factors for the coordinates ξ_1, ξ_2, and ξ_3.
The other components of $(\vec{B}\cdot\nabla)\vec{A}$ are found by cyclic permutation of the
subscripts of Eq. (4) (see Ref. 20).

If circular cylindrical coordinates are taken for the generalized
coordinates, the scale factors become h_r = 1, h_θ = r, and h_z = 1. The
components of $(\text{M}\cdot\nabla)\text{H}$ are then found to be

$$\left[\left(\vec{M}\cdot\nabla\right)\vec{H}\right]_r = M_r\ \frac{\partial H_r}{\partial r} + \frac{M_\theta}{r}\ \frac{\partial H_r}{\partial \theta} + M_z\ \frac{\partial H_r}{\partial z} - M_\theta\ \frac{H_\theta}{r}$$

$$\left[\left(\vec{M}\cdot\nabla\right)\vec{H}\right]_\theta = \frac{M_\theta}{r}\ \frac{\partial H_\theta}{\partial \theta} + M_z\ \frac{\partial H_\theta}{\partial z} + M_r\ \frac{\partial H_\theta}{\partial r} + M_\theta\ \frac{H_r}{r} \tag{5}$$

$$\left[\left(\vec{M}\cdot\nabla\right)\vec{H}\right]_z = M_z\ \frac{\partial H_z}{\partial z} + M_r\ \frac{H_z}{\partial r} + \frac{M_\theta}{r}\ \frac{\partial H_z}{\partial \theta}\ .$$

When the bias field is applied to the ferrofluid in the prototype sound projector, the only non-zero components of M and H are those in the azimuthal direction. Since the azimuthal magnetic field is constant in the azimuthal direction, the only non-zero component is

$$[(M\cdot\nabla)H]_r = - M_\theta\ \frac{H_\theta}{r}\ . \tag{6}$$

So, the magnetic body force term for the prototype sound projector is

$$\mu_o(\vec{M}\cdot\nabla)\vec{H} = -\mu_o\ M_\theta\ \frac{H_\theta}{r}\ \hat{e}_r\ . \tag{7}$$

The azimuthal magnetic field, therefore, results in a radial force. The equation of motion in the r direction is then

$$\rho\left[\frac{\partial v_r}{\partial t} + V_r\ \frac{\partial v_r}{\partial r} + \frac{v_\theta}{r}\ \frac{\partial v_r}{\partial \theta} - \frac{v_\theta^2}{r} + V_z\ \frac{\partial v_r}{\partial z}\right] = -\ \frac{\partial p}{\partial r} - \mu_o M_\theta\ \frac{H_\theta}{r}\ . \tag{8}$$

Because of the radial symmetry of the geometry v_θ and $\partial v_r/\partial \theta$ are equal to zero. The advective acceleration may be ignored, thus reducing the equation of motion to

$$\rho\ \frac{\partial v_r}{\partial t} = -\ \frac{\partial p}{\partial r} - \mu_o\ M_\theta\ H_\theta/r\ . \tag{9}$$

The equation of conservation of mass simplifies to

$$rv_r(r) = \text{constant}. \tag{10}$$

B. Nonlinear Behavior

As stated in Chapter I, the purpose of the bias field was to avoid nonlinearities in the response of the transducer. The magnetization curve of the ferrofluid (Fig. 1) can be approximated by the straight lines shown in Fig. 9. If the operating point of the transducer is chosen in the region of Fig. 9 marked "A", then the magnetization of the ferrofluid will be directly proportional to the magnetic field intensity. According to Eq. (7) the body force in the ferrofluid is proportional to $M_\theta H_\theta$. If $H_\theta = H\cos\omega t$ and K is the factor of proportionality between the magnetization of the ferrofluid and the magnetic field intensity, then the magnetization can be written

$$|M| = KH_\theta \cos\omega t , \tag{11}$$

and the resulting force is given by

$$\vec{f} = \frac{\mu_o K H_\theta^2}{r} \left[\frac{1}{2} + \frac{1}{2}\cos 2\omega t\right] \hat{e}_r . \tag{12}$$

The resulting force is the second harmonic of the driving signal voltage.

The magnetization in region B is approximately constant with magnetic field intensity so that $|M| = M_o$ where M_o is the saturation magnetization. The resulting body force in the ferrofluid for operation in this region is given by

$$\vec{f} = \mu_o M_o \frac{H_\theta}{r} \cos\omega t \, \hat{e}_r , \tag{13}$$

17

and is at the same frequency as the driving signal voltage. Region B of Fig.
13 is, therefore, the desirable region for the operating point. In deciding
on the optimal value for the magnetic bias field, one should take into account
that the gaps between the two toroid halves cause a decrease in the nominal
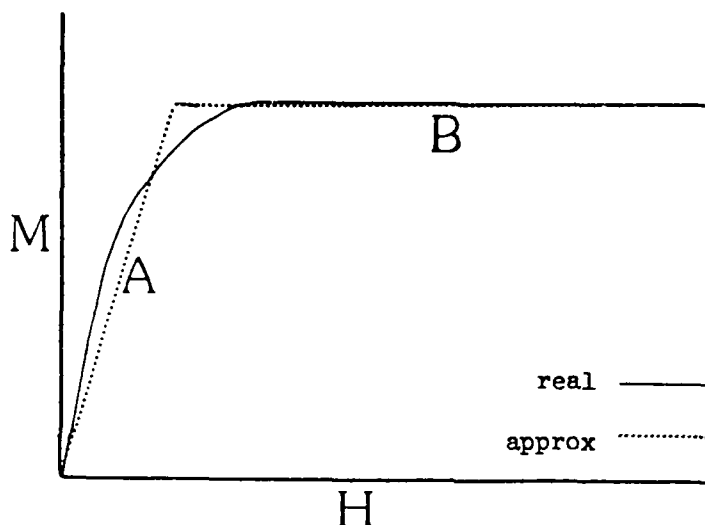field strength of about 6%.

Fig. 9 - Approximation to the magnetization curve

C. Electroacoustic Transduction

The ferrofluid projector may be considered as a nonideal transformer with
a moving core. The problem may be considered as a 3-port electromechanical
network, governed by the following set of equations:

$$e_1 = L_1 \frac{di_1}{dt} + M \frac{di_2}{dt} + kT_1 v \ , \tag{14a}$$

$$e_2 = M \frac{di_1}{dt} + L_2 \frac{di_2}{dt} + kT_2 v \ , \tag{14b}$$

$$F = kT_1 i_1 + kT_2 i_2 + Z_m v \ , \tag{14c}$$

where $e_{1,2}$ = voltage across coil 1,2,

$\quad$ $i_{1,2}$ = current in coil 1,2,

$\quad$ $L_{1,2}$ = self-inductance of coil 1,2,

$\quad$ $T_{1,2}$ = transfer coefficients,

$\quad\quad$ M = mutual inductance between coils,

$\quad\quad$ Z_m = mechanical impedance of ferrofluid cavity (including fluid loading),

$\quad\quad$ F = external force applied to outer elastomer wall,

$\quad\quad$ v = velocity of outer elastomer wall, and

$\quad\quad$ k = spatial operator relating the direction of F to i and e to v, $k^2 = -1$.

Coil 1 is taken as the modulation coil while coil 2 is the bias coil.

The two coils are assumed to be perfectly coupled; all the magnetic flux that passes through one also passes through the other. This assumption leads to the equations $M = \sqrt{L_1 L_2}$ and $L_1/L_2 = (N_1/N_2)^2$, where N_1 and N_2 are the number of turns of coil 1 and 2, respectively.

The transfer coefficient T_1 is defined as the ratio between e_1 and v while $i_1 = i_2 = 0$, which implies $H = 0$. Since the ferrofluid is in the saturated state, one finds for the magnetic induction
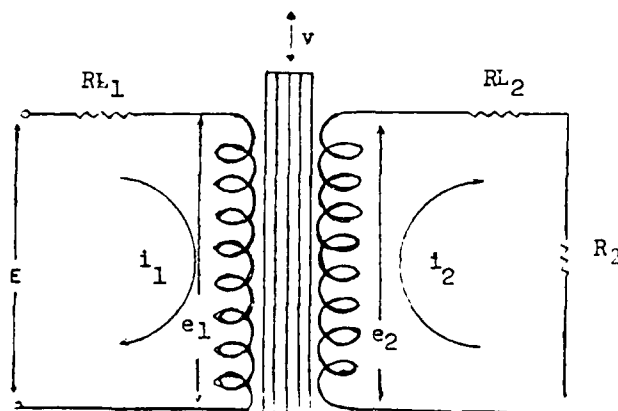
$$\vec{B} = \mu_o \vec{M}_o \ , \tag{15}$$

and the magnetic flux is given by

$$\Phi = \mu_o M_o h (r_2 - r_1) \, , \tag{16}$$

where r_1 and r_2 are the radii of inner and outer walls of the cavity, respectively, and h is the height. The flux varies because of the time dependence of r. Thus, the induced voltage in the first coil is ($v_2 \equiv v$)

$$e_1 = - N_1 \frac{d\Phi}{dt} = \mu_o M_o N_1 h (v_1 - v_2) \, . \tag{17}$$

v = velocity of ferrofluid cavity outer wall,

e = inductive voltages across coils,

i = electrical currents in coils,

R_L = ohmic resistance of coils,

E = driving voltage, and

R_2 = closing resistance.

Fig. 10 - Equivalent transformer for toroid

Using Eq. (17) one finds for the transfer coefficient T_1

$$T_1 = \frac{e_1}{v_2} = \mu_o M_o N_1 h \left[\frac{r_2 - r_1}{r_1} \right] \, , \tag{18}$$

20

and

$$T_2 = (N_2/N_1)T_1.$$ (19)

The same transfer coefficients may be derived as ratios between force and currents i_1 and i_2 by the reciprocity implicit in Eq. (19). This may be confirmed by integrating the force per unit volume, Eq. (7), between r_1 and r_2.

The mechanical impedance Z_m of the ferrofluid cavity is the ratio of the force on the cavity to the velocity of the outer elastic wall in the absence of current i_1, i_2. The mechanical impedance will have lumped inductive, capacitive, and resistive elements. The inductive components of the mechanical impedance result from the equivalent mass of the ferrofluid cavity. The capacitive component results from the elasticity of the cavity's rubber walls. The resistive component results from mechanical friction as well as radiation resistance from the surrounding water. The elastic and resistive components can be accounted for with K and R_m, a lumped elasticity/unit area constant and a lumped resistance/unit area constant. The mass term must account for the mass of the ferrofluid as well as the effective mass of the water moved by the oscillation of the ferrofluid.

The mass component of the mechanical impedance can be derived by considering the pressure difference across the ferrofluid cavity outer wall. The force on the outer wall is given as

$$F = (p_3 - p_2) \cdot A$$ (20)

where p_3 = pressure just outside outer cavity wall,

p_2 = pressure just inside outer cavity wall, and

A = outer wall area.

The value of p_2 can be found by considering Euler's equation and ignoring convective acceleration

$$-\frac{\partial p}{\partial r} = \rho_f \frac{\partial v(r)}{\partial t} \, , \qquad (21)$$

where ρ_f = density of the ferrofluid and

$v(r)$ = velocity at radius r.

Using Eq. (10), Eq. (21) can be integrated to yield

$$-p_2 + p_1 = j\omega\rho_f v r_2 \ln(r_2/r_1) = j\omega m_f v, \qquad (22)$$

where p_1 = pressure just inside inner cavity wall,

v = velocity of outer cavity wall, and

m_f = effective mass of ferrofluid/unit area of outer wall,

so that

$$m_f = \rho_f r_2 \ln(r_2/r_1). \qquad (23)$$

Because of the pressure-release surface at the transducer's inner wall, $p_1 = 0$; therefore,

$$- p_2 = j\omega m_f v. \qquad (24)$$

The loading by the acoustic medium is accounted for in the expression for p_3. The geometry of the test tank makes a rigorous solution for the water load on the transducer's active surface impractical.

An order of magnitude estimate is obtained as follows. The transducer's active surface is replaced with a sphere of equal surface area with radius r_3. The outer surface of the water (at the walls of the box and the free surface) is replaced by a sphere with radius r_4. The values of r_3 and r_4 are given by the relations

$$r_3 = \sqrt{\frac{r_2 h}{2}} \qquad (25)$$

$$r_4 = \sqrt{\frac{xy + xz + yz}{2\pi}} \qquad (26)$$

where x, y, and z are the dimensions of the water in the box (84×88×15 cm^3).
The continuity equation for this system yields

$$v(r) = v_3 \left(r_3/r \right)^2 . \qquad (27)$$

Using Eq. (27), Euler's equation now yields

$$- p_4 + p_3 = j\omega\rho_o v_3 r_3^2 \left[\frac{r_4 - r_3}{r_3 r_4} \right] , \qquad (28)$$

where ρ_o is the density of the water in the tank. The sides and bottom of the
box act approximately as pressure-release surfaces so that $p_4 = 0$ leading to

$$p_3 = j\omega m_a v , \qquad (29)$$

where $v = v_3$, the velocity at the outer wall of the cavity, which in turn is
equal to v_2 defined before by virtue of the assumed continuity of volume
velocity. The effective mass of the loading by the water in the box m_a is
given by

$$m_a = \rho_o \ (r_3/r_r) \ (r_4 - r_3). \qquad (30)$$

The force on the outer cavity wall is found from Eqs. (20), (24), and (30) to
be

$$F = j\omega(m_a + m_f)v \cdot A . \qquad (31)$$

Using the constants K and R_m, the mechanical impedance of the ferrofluid cavity is then

$$Z_m = \frac{F}{v} = \left[j\omega(m_a + m_f) + \frac{K}{j\omega} + R_m \right] 2\pi r_2 h \; . \tag{32}$$

For most of the analysis presented in this report, it will be assumed that the capacitive and resistive portions of the mechanical impedance are negligible compared with the inductive portion; therefore,

$$Z_m = j\omega(m_a + m_f) 2\pi r_2 h \; . \tag{33}$$

For the experimental setup used, the values of r_3, r_4, m_a, and m_f are $r_3 =$ 0.084 m, $r_4 = 0.454$ m, $m_a = 68.5$ kg/m^2, and $m_f = 74.4$ kg/m^2.

D. Solution for Acoustic Field in Test Tank

The transduction Eqs. (14) may be solved for the case of the projector in operation by noticing that in regular operation the bias coil is connected to the rectifier, which is considered to an ohmic resistance R_2. There is no external force on the cavity wall not already accounted for in Z_m; thus, F = 0. Solution of the set of linear Eqs. (14) results in

$$\frac{1}{Z_1} = \frac{i_1}{e_1} = \frac{1}{\left(j\omega L_1 \right) + \left(T_1^2 / Z_m \right)} + \frac{1}{\left(N_1/N_2 \right)^2 R_2} \; , \tag{34}$$

and

$$\frac{v}{e_i} = \frac{- kT_1}{j\omega L_1 Z_m + T_1^2} \; . \tag{35}$$

The total input impedance to the first coil Z should include the resistance of the coil, R_{L1}, and thus $Z = Z_1 + R_{L1}$. The relation between the voltage E applied to coil 1 and the resulting velocity v of the outer wall of the cavity is then

$$\frac{v}{E} = -\frac{kT_1}{j\omega L_1 Z_m + T_1^2}\left[\frac{Z_1}{Z_1 + R_{L1}}\right] .\tag{36}$$

The velocity $v(r)$ at an arbitrary distance from the cavity wall is given by

$$v(r) = v\left(r_3/r\right)^2 ,\tag{37}$$

and the pressure at distance r is

$$p(r) = j\omega\rho_o vr_3^2\left[\frac{r_4 - r}{vr_4}\right] .\tag{38}$$

Of course, it should be kept in mind that these expressions follow from the highly idealized spherical geometry assumed in place of the rectangular test tank.

The value of p at a distance r = 0.27 m, according to Eq. (38) with v from Eq. (36), is shown in Fig. 15.

E. Estimate of Results for Operation in an Infinite Medium

The analysis will be simplified by approximating the radiating surface of the prototype with a spherical surface of equal area. The radiation loading of an oscillating sphere is determined by its specific acoustic impedance Z_o, defined by $p(r_3) = Z_o v(r_3)$, where r_3 is the radius of the surface of the sphere. The specific acoustic impedance can be divided into a resistive portion, r_o, and a reactive position, m_o, such that $Z_o = r_o - j\omega m_o$. Expressions for the radiation resistance r_o and the accession to inertia m_o are given in Ref. 21 as

$$r_o = \frac{\rho c \left(kr_3\right)^2}{\left[\left((kr_3)^2 + 1\right)\right]} , \tag{39}$$

and

$$m_o = \frac{\rho r_3}{\left[\left(kr_3\right)^2 + 1\right]} , \tag{40}$$

where c is the speed of sound and k is the wave number $2\pi/\lambda$. In the low-frequency limit $(kr_3)^2 \ll 1$ and these expressions reduce to $r_o \cong \rho c(kr_3)^2$ and $m_o \cong \rho r_3$. Taking the ratio $(r_o/\omega m_o) = kr_3$, it is apparent that at low frequencies $(kr_3 < 1)$, the radiation resistance is negligible compared with the accession to inertia. Using the value for r_3 calculated in the last section, the accession to inertia for the prototype is $m_o \cong \rho r_3 = (1000 \text{ kg/m}^3)(0.084 \text{ m}) = 84 \text{ kg/m}^2$ which is, considering the approximations used in this analysis, nearly the same as the fluid loading calculated for the test tank (where $m_a = 68 \text{ kg/m}^2$). Thus, one would feel warranted to assume that the pressure near the projector in a free-field situation is about the same as that near the projector in the test tank.
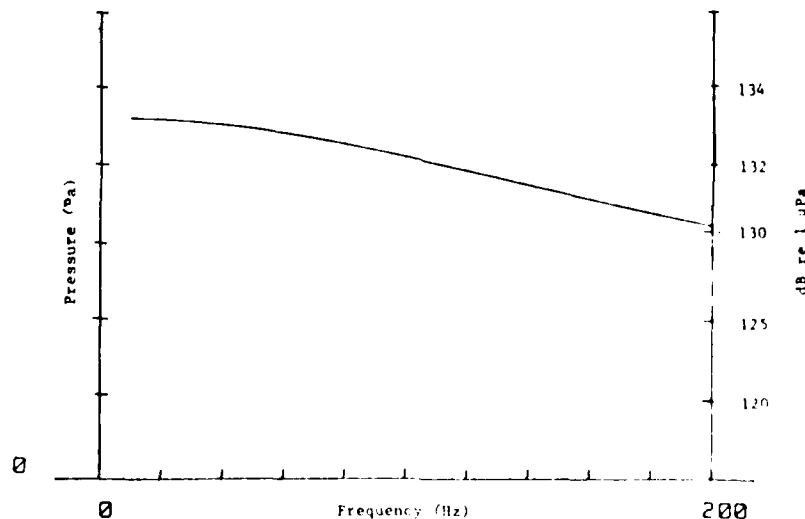

Fig. 11 - Pressure at intermediate distance vs frequency for E = 60 V

In order to predict the total power emitted in a free-field situation,
one could use the pressure measured in the test and find the power P by

$$P = 4\pi r^2 \ [p(r)]^2/(\rho c). \tag{41}$$

IV. EXPERIMENTAL INVESTIGATION

A. Introduction

The prototype projector described in this report was built for the larger
part at the Underwater Sound Reference Detachment of the Naval Research
Laboratory (NRL-USRD). Part of the building and testing was done at the
Florida Institute of Technology. The need for a large dc was the most
difficult to satisfy. The power supply used was a type APS-20 Mallory
Rectostarter. Wire gauge larger of at least #4 was needed to handle the
current.

The calculations with respect to impedance, transfer coefficients, and
field strengths presented in Chapter III may be tested on the prototype.
Measurements were performed of impedance with the dc supply and open-
circuited. The magnetic field strength was also measured under these
circumstances. In general, the measurement results concurred well with the
computations, in magnitude and in frequency dependence. Details are given in
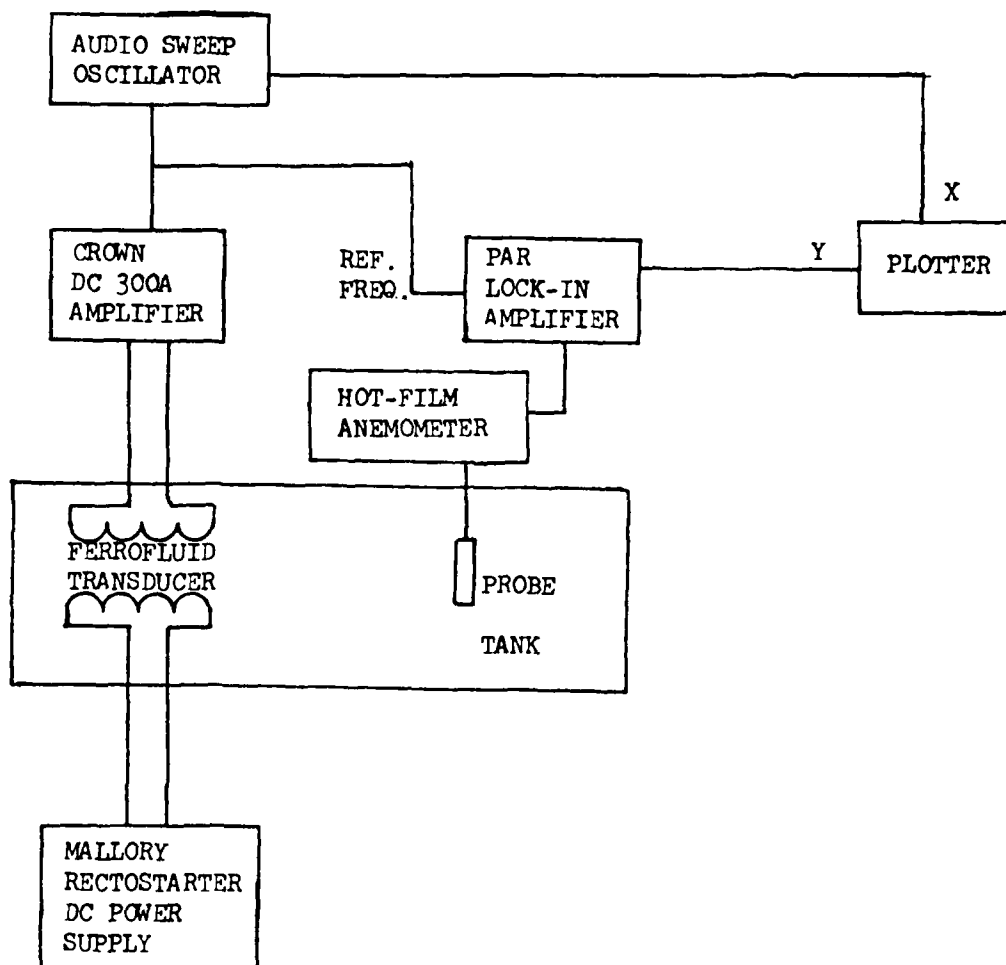Ref. 22.

Fig. 12 - Swept frequency measurement setup

B. Acoustical Output Data

The prototype transducer output was measured with an NRL-USRD type F61 hydrophone and with a hot-film anemometer technique [23]. The experimental setup used with the F61 hydrophone is shown in Fig. 16. The hydrophone output is measured with a Princeton Applied Research Lab Model 129 lock-in analyzer. The hydrophone had to be shielded from electromagnetic interference with a grounded copper screen shield. Without the shield, the stray electric currents in the water completely masked the acoustic signal. The sensitivity of the F61 hydrophone is -205.5 dB re 1 V/μPa.

The results of the measurements are shown in Figs. 13 through 19. The abscissa is the frequency of the ac excitation voltage. Thus in the case of the measurements of pressure at twice the frequency (Figs. 13 and 14), the measured frequency is twice the value read on the horizontal axis.

It appears that the noise background is about the same for the corresponding cases of bias field on and bias field off. The alleged signal in Figs. 13, 17, 18, and 20 consists of a series of resonances.

In Chapter III, Section B, it was predicted that the acoustic output of the prototype sound projector would occur at twice the frequency of the ac modulation voltage if no bias field were applied to the prototype. Figures 13 and 14 show the acoustic output at twice the driving voltage frequency for the cases where the bias field is present (Fig. 14) and where it is absent (Fig. 13). Comparing these figures, one can see that several of the resonances that appear in Fig. 13 are not present in Fig. 14, most noticeably the peaks at 46 and 23 Hz. These peaks indicate that the prototype is generating sound at the second harmonic without the bias field, and this sound disappears when the bias field is applied. Further support for this interpretation can be found in Fig. 15, which shows that the resonances in Fig. 13 decrease with decreasing modulation coil current. Notice that the resonance at 30 Hz is present in all three figures and does not vary with modulation-coil current. The fact would indicate that this feature results from 60-Hz induction.

Figures 16 through 18 show the acoustic output of the prototype at the same frequency as the driving voltage. Figures 16 and 17 show the output for the cases where the bias field is present (Fig. 17) and where it is absent (Fig. 16). As one would expect from the theory developed in Chapter III, the presence of the bias field has a significant effect on the acoustic output of the prototype. It should be remembered that the current available for the bias field in the experiment was not quite enough to bring the ferrofluid fully to saturation. This fact may explain why the experimental values for acoustic output fall short of the theoretical predictions over most of the range of frequencies measured.
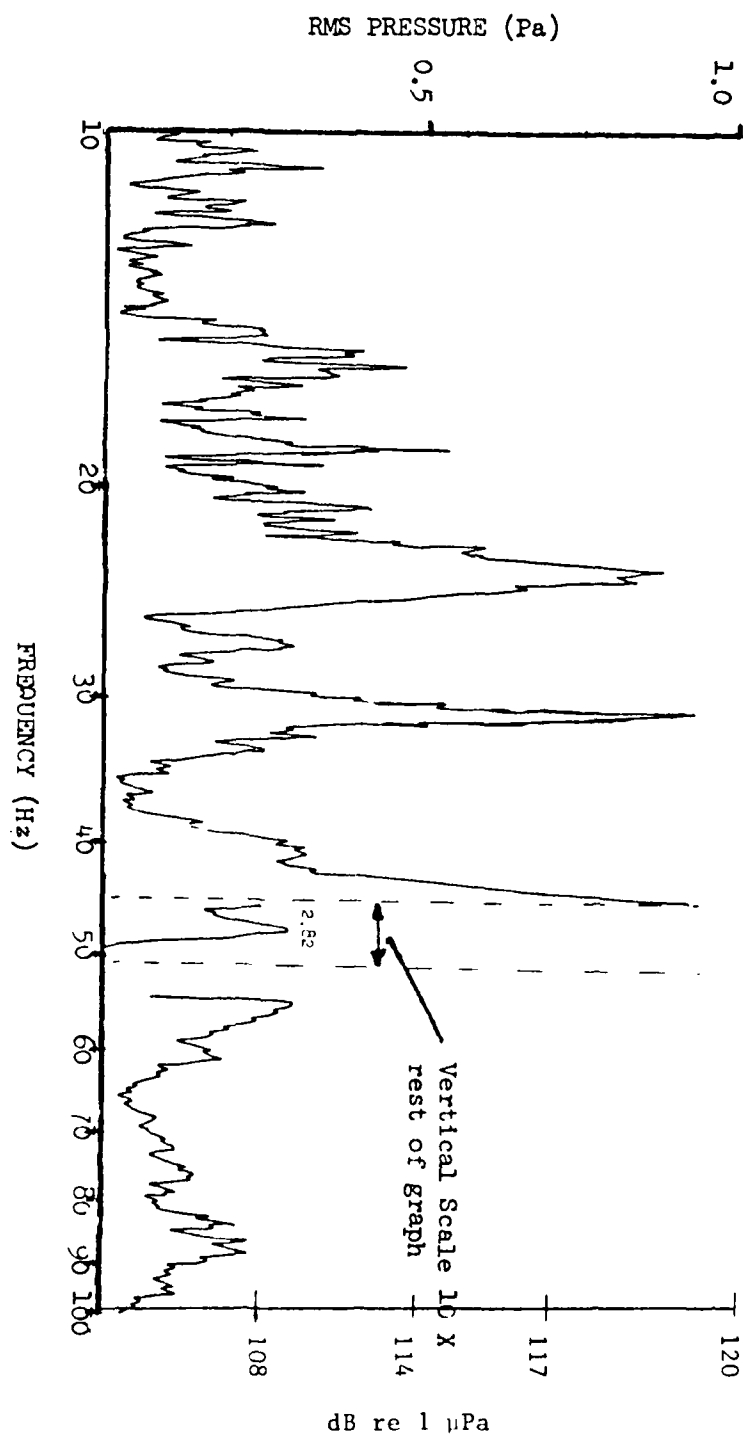
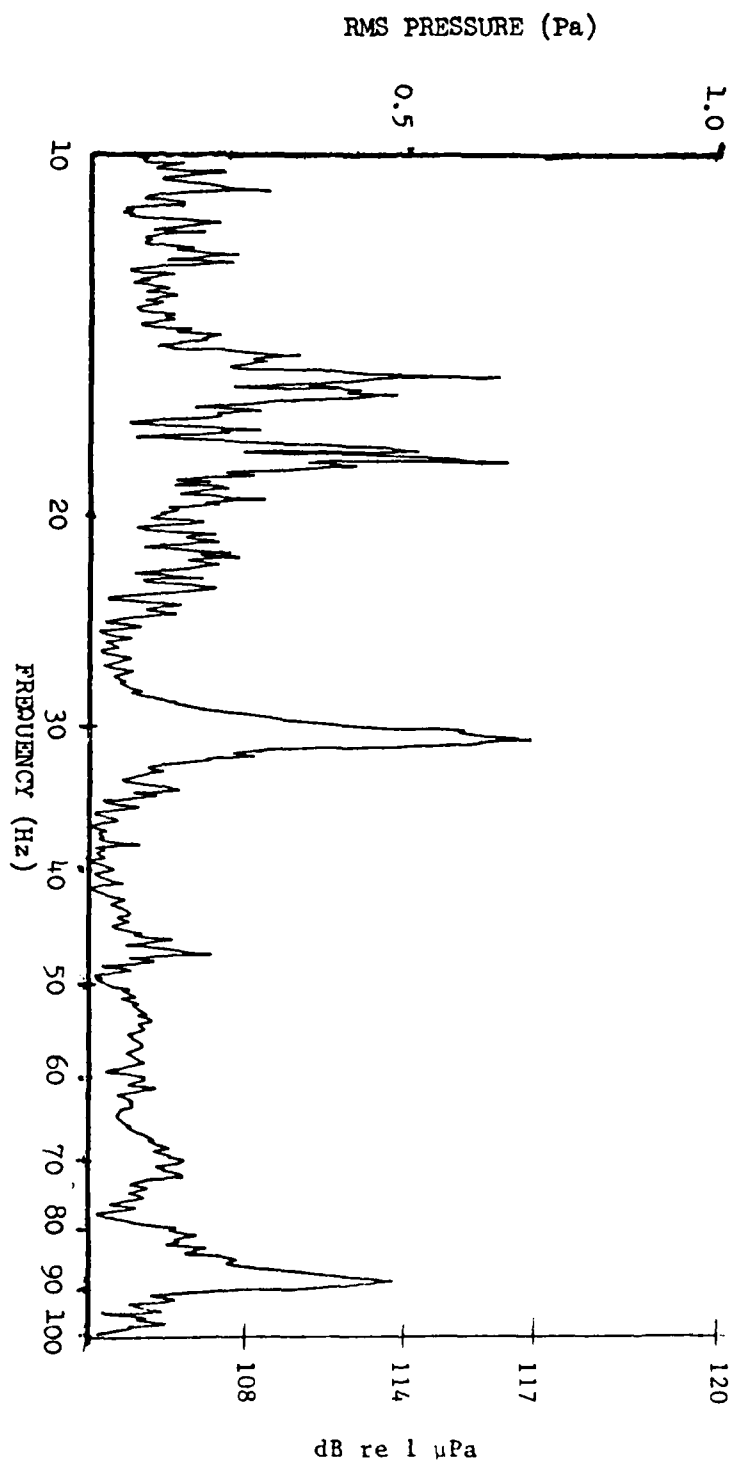Fig. 13 - Acoustic output at 2f with bias field off

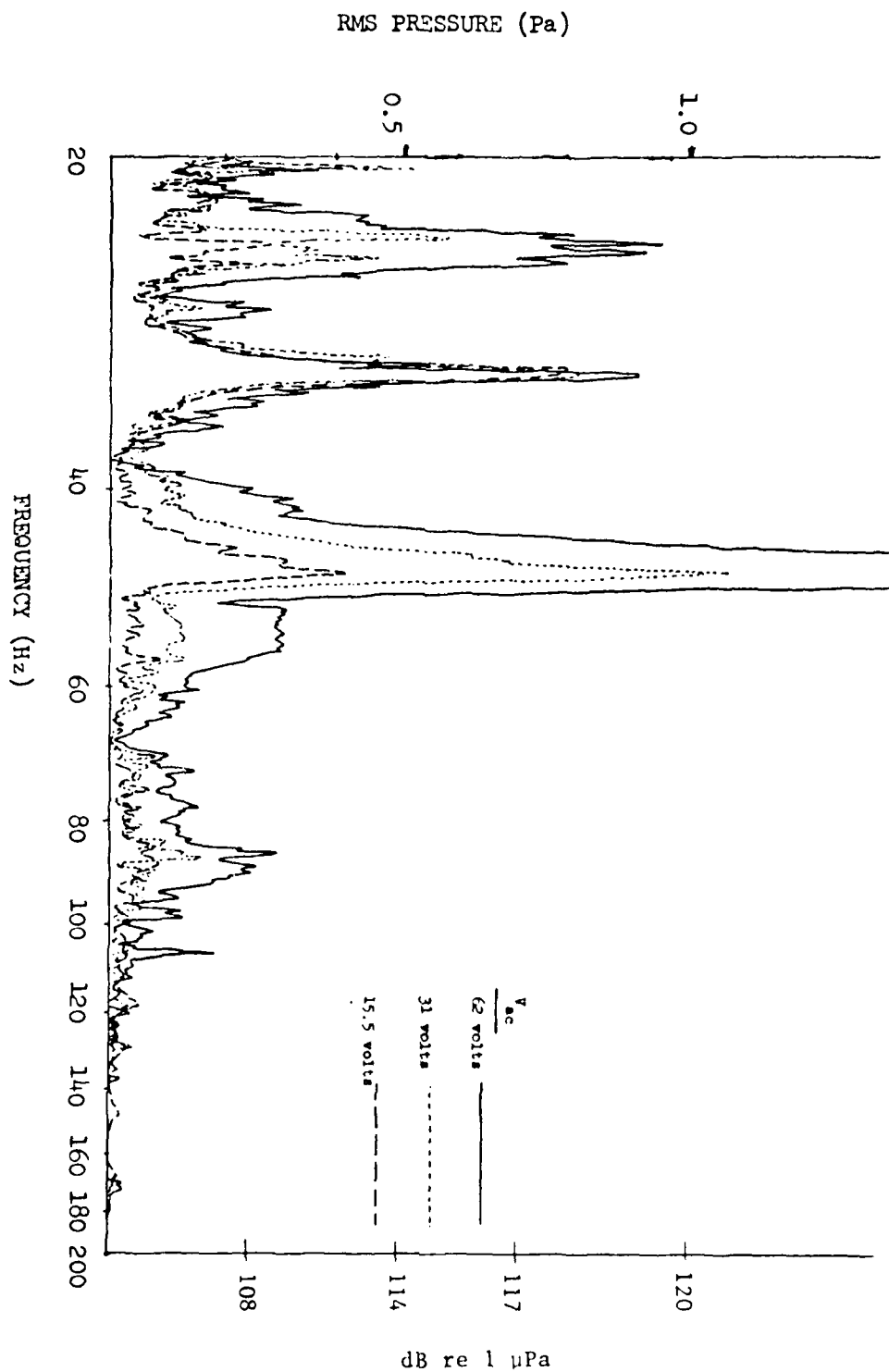Fig. 14 - Acoustic pressure output at 2f with bias field on

RMS PRESSURE (Pa)

Fig. 15 - Acoustic output at 2f for various levels of modulation field with
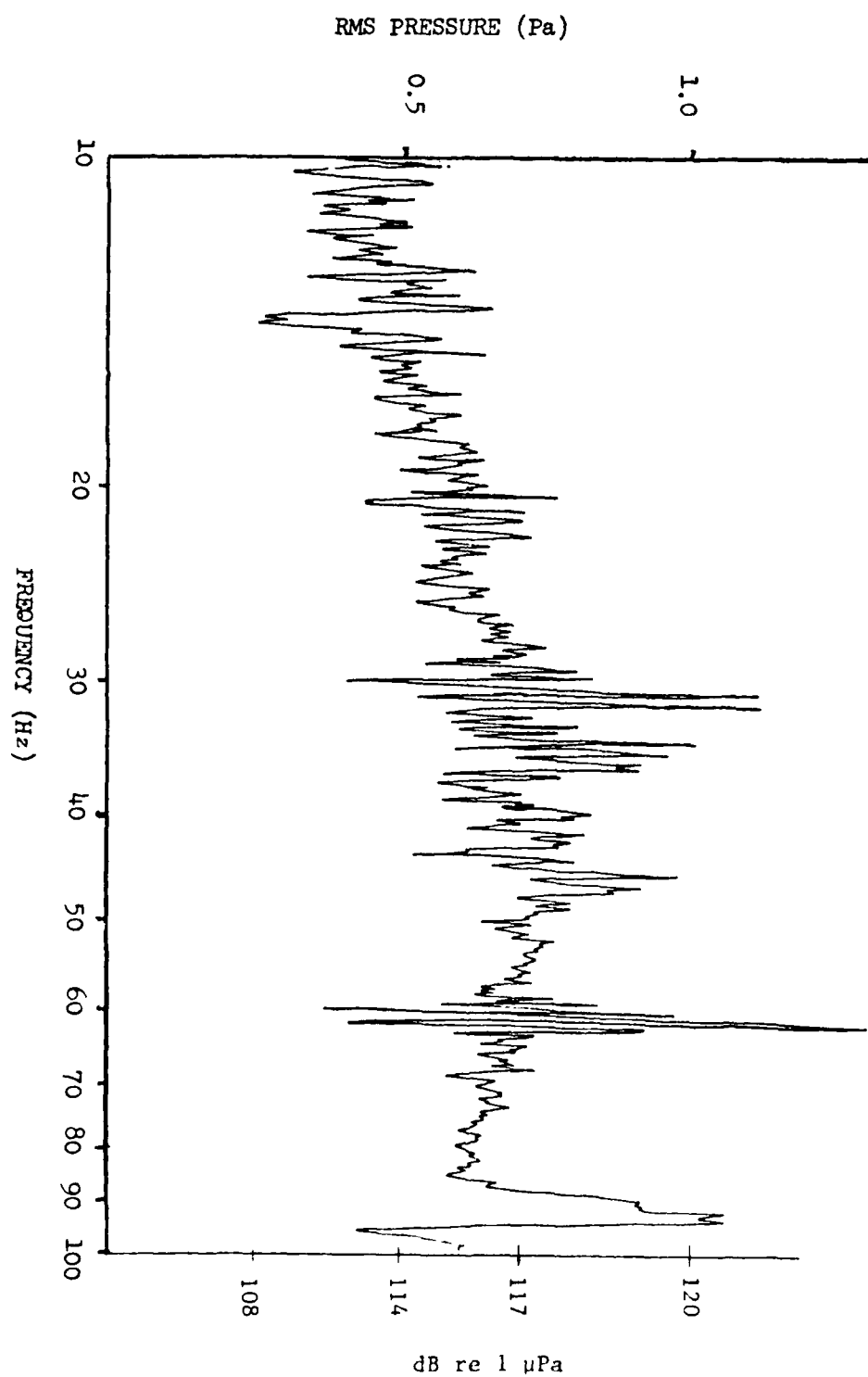   bias field off

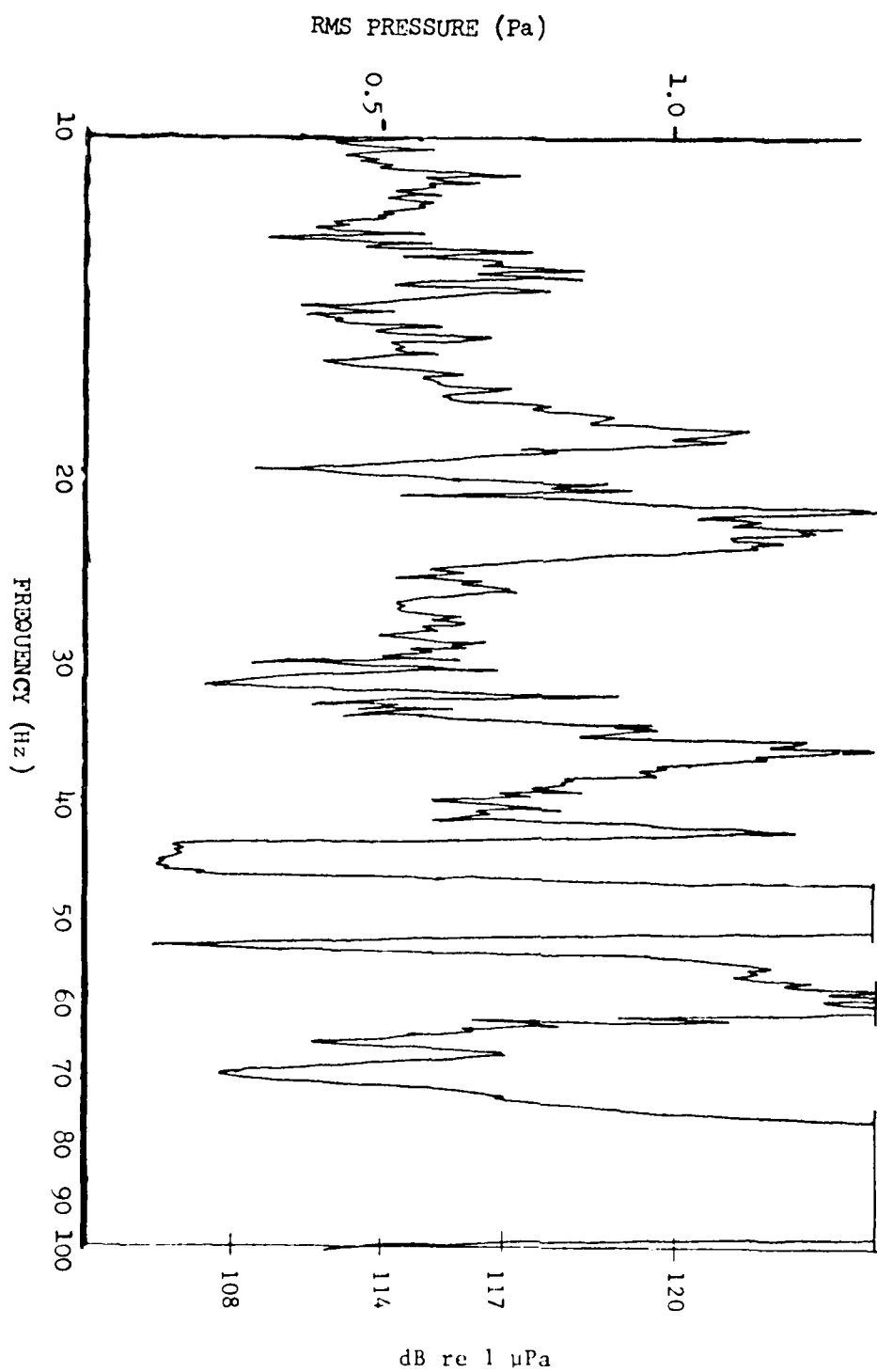Fig. 16 - Acoustic output at 1f with bias field off

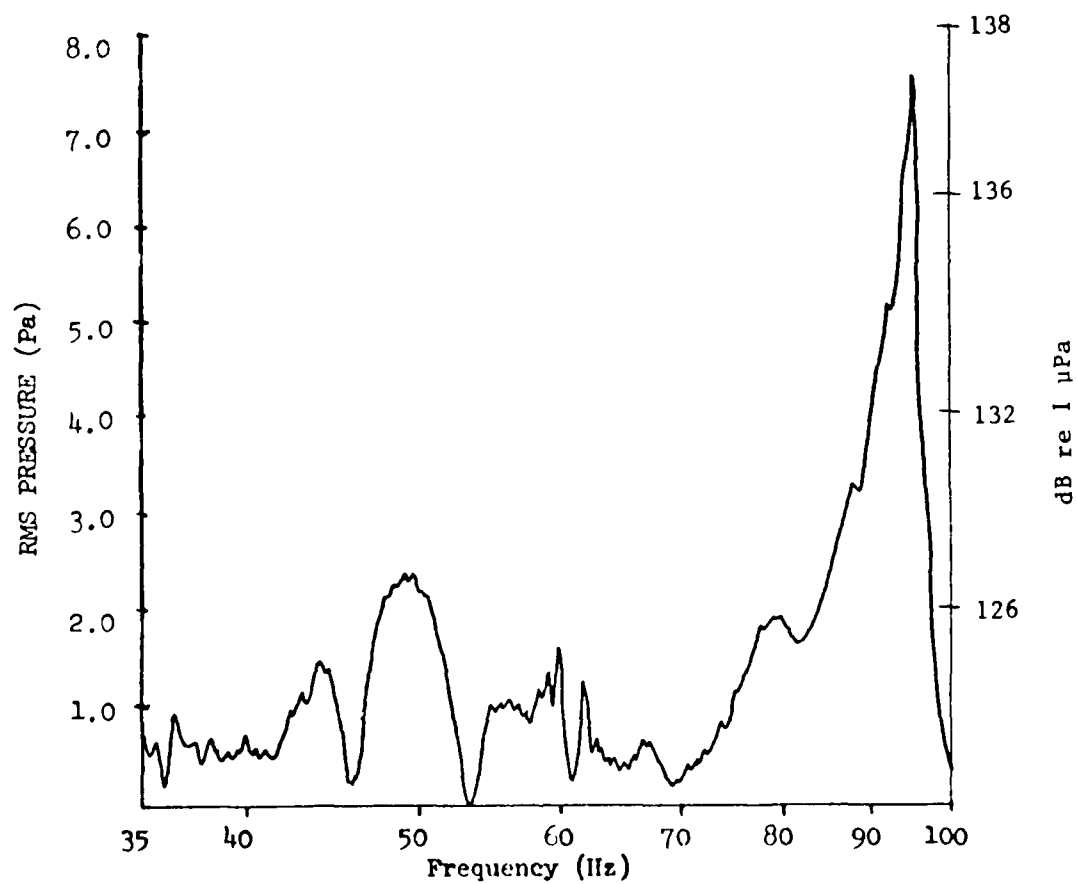Fig. 17 - Acoustic output at 1f with bias field on

Fig. 18 – Same as Fig. 17 with expanded vertical scale

Table I is a key to the acoustical measurement data and can be used to facilitate comparisons among the various plots.

Table I - Measurement Index

	Bias Field Off	Bias Field On
Measurement at Driving Voltage Frequency	Fig. 16 Fig. 19	Fig. 17 Fig. 18 (Expanded Vertical Scale) Fig. 20
Measurement at Twice Driving Voltage Frequency	Fig. 13 Fig. 15 (Various Levels of Driving Voltage)	Fig. 14

In general, the measured pressure is an order of magnitude lower than the values computed and shown in Fig. 10 on the basis of numerical parameters. The operating point and ac voltage, though, were lower.

If one derives typical value of 0.6 Pa for the pressure between 10 and 40 Hz at a distance of 0.27 m, one may derive a total power P predicted for free-field operation of $P = 0.2$ μW. Of course, this assumes that the observed signal originates in the ferrofluid.

C. Hot-Film Anemometry Results

A second approach, which was used to verify the low-frequency operation of the prototype, was a hot-film anemometry technique (Ref. 23). The technique uses the cooling of a heated film to detect acoustic particle motion. The value of this technique lies in its increased sensitivity to low-

frequency hydroacoustic fields. Moreover, the input resistance of this device is low, and thus it is insensitive to the stray currents in the water.

The probe used was a TSI, Inc. Model 1210-20W standard straight probe. The probe was located near the surface midway between the prototype sound projector and the tank wall and was oriented to detect vertical particle motion. The sound projector would cause the water in the tank near the surface to oscillate vertically as a result of the pressure-release boundary.

The curve in Fig. 19 was taken with the prototype operating without a bias field while that in Fig. 20 was taken when the bias field was applied. The difference in temperature between the sensor and the undisturbed medium was 30°C.
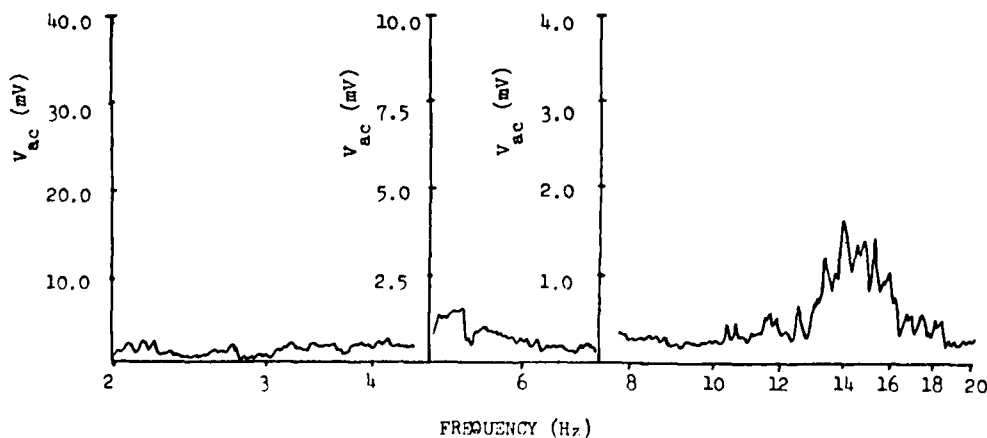

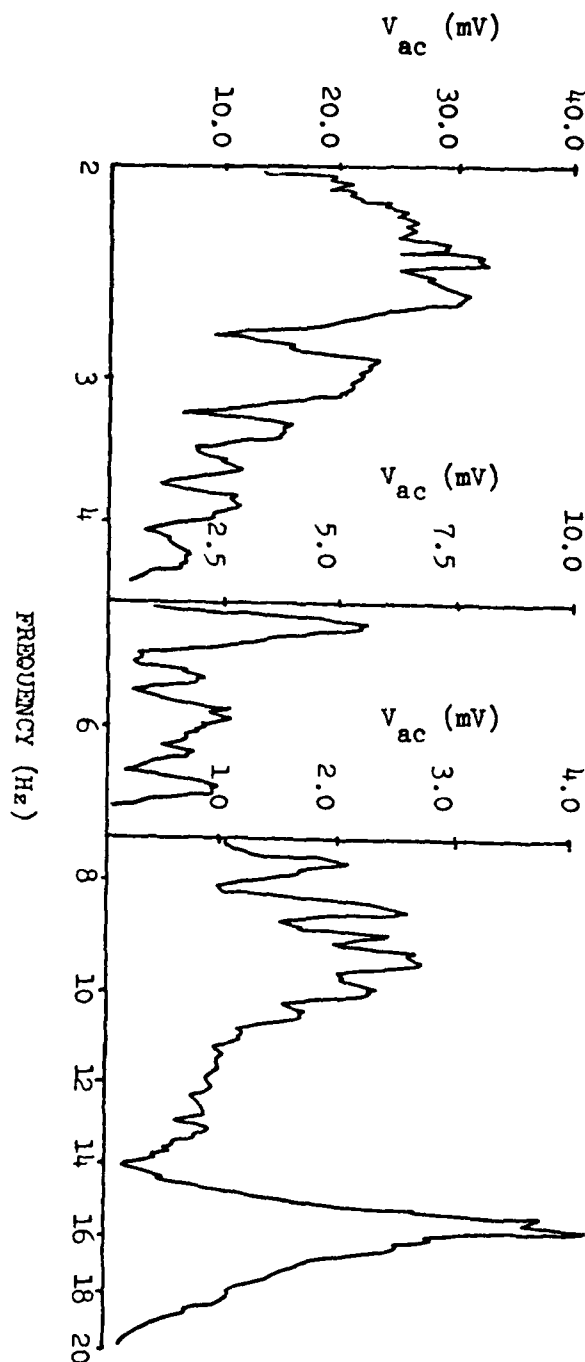Fig. 19 - Hot-film anemometry measurement without bias field

Fig. 20 - Hot-film anemometry measurement with bias field applied

Table II. Hot-Film Anemometry Measurement Results

	Without Bias		With Bias	
Frequency (Hz)	V_{ac} (mV)	Particle Velocity ($\mu m/s$)	V_{ac} (mV)	Particle Velocity ($\mu m/s$)
2.0	1.0	2.6	15.0	39.0
3.0	0.5	1.9	22.0	85.8
4.0	2.5	13.0	5.0	26.0
6.0	0.6	4.7	1.75	13.7
8.0	0.3	3.1	2.00	20.8
10.0	0.2	2.6	2.0	26.0
12.0	0.3	4.7	0.9	14.0
14.0	1.5	27.3	0.1	1.8
16.0	1.0	20.8	3.0	62.4
18.0	0.3	7.0	1.0	23.4
20.0	0.2	5.2	0.1	2.6

In Table 14 of Ref. 23 one finds the value for the coefficient a in the relationship between the ac Nusselt number Nu_{ac} and the relative displacement ς/d, where d is the diameter of the sensor. One has a = 0.108, Nu_{ac}/V_{ac} = 0.447, and d = 50 μm. This leads to the following relation between V_{ac} and w (vertical velocity) w(mm/s) = $0.00130f(Hz)V_{ac}(mv)$, where f is the frequency. Table II gives the values for the output voltage V_{ac} and the computed particle velocity.

To compare the anemometer results with the pressure measurements, one may use Eq. (38) for p(r). Assuming that p(r) is measured at an intermediate point r = $(r_3 + r_4)/2$, it follows that the measured pressure amplitude p_m is

$$p_m = \omega\rho \, v_3 r_3^2 \, \frac{r_4 - r_3}{(r_4 + r_3) \, r_4^2} \, . \tag{42}$$

On the other hand the velocity measured at the surface r_4 follows from

$$v_4 = v_3 \, (r_3/r_4)^2, \tag{43}$$

and

$$p_m = v_4 \omega\rho \, \frac{(r_4 - r_3)}{(r_4 + r_3)} \, . \tag{44}$$

The hot-film anemometry calibration gave

$$v_4(m/s) = 0.130 \times 10^{-6} \, [f(Hz)] \, V_{ac}(mv), \tag{45}$$

and thus

$$p_m(Pa) = 0.56 \times 10^{-3} [f(Hz)]^2 V_{ac}(mv). \tag{46}$$

The value of V_{ac} measured by hot-film anemometry is considerably lower than would follow from this relation between p_m and V_{ac} if one inserts the values for p_m found by the pressure hydrophone.

V. CONCLUSIONS AND RECOMMENDATIONS

A. Conclusions

The acoustic pressure measurements made with the NRL-USRD type F61 standard hydrophone and the acoustic particle motion measurements made with the hot-film anemometry technique both suggest that the prototype ferrofluid hydroacoustic projector is capable of producing low-frequency underwater sound. The major features of the prototype operation predicted by the theory

presented in Chapter III were observed in the experimental data. Second
harmonic acoustic output was observed when the prototype was operated without
a bias field. The bias field was also shown to have a significant effect on
the acoustic output signal amplitude at the first harmonic of the driving
frequency.

The resonances observed in the graph for pressure and particle velocity
could be due to flexural wave resonances in the walls of the wooden tank. The
flexural wavespeed in 1/4-in. thick wood is quite low and of the right
magnitude to cause standing waves of various frequencies, due to the spread in
dimensions of the faces of the tank.

It is improbable that these resonances originate in the ac coils, dc
coils, or aluminum frame since their vibrations would not be accompanied by
volume changes and thus have poor coupling to the tank medium. Still, it
would be worthwhile to confirm the assumption in that the sound originates in
the ferrofluid by replacing the latter by a non-magnetic fluid and repeating
the measurements.

The experimental results obtained were greatly affected by the available
equipment. In principle, the only limit to the acoustic power output of the
prototype is the current handling ability of the coils and the available
sources of power. With the proper design, a ferrofluid transducer would be
able to deliver large amounts of low-frequency acoustic power that would
otherwise be unavailable.

B. Recommendations

The following recommendations are made for the continuation of this
project.

1. Repeat the measurements in a nonresonant environment. The data
presented in this study are difficult to interpret due to the presence of
so many resonances. Data taken in a nonresonant environment would allow a

better check on the frequency response of the prototype. Measurements
with a non-magnetic fluid instead of ferrofluid would be a good check on
the validity of the observed signal.

2. Ferrofluids with higher saturation magnification. Waterbase
ferrofluids with saturation magnetizations larger than 140 G are
commercially available. Use of such fluid is expected to greatly increase
the output of the projector.

3. Elimination of the modulation coil. The present study shows that the
presence of two separate coils for modulation and bias field generation
results in a transformer action that reduces the magnetic fields necessary
for sound generation. It is, therefore, desirable to eliminate one of the
coils. One approach would be the use of the permanent magnets mentioned
in item 4. Another approach would be to modulate the bias current in the
bias coil with a transformer.

4. Use of permanent magnets in bias field generation. The need for a
large bias current is one of the major drawbacks to this design. The
power generated by the dc power supply does not contribute directly to the
acoustic output and thereby decreases the overall efficiency of the
design. It may be possible to generate the required bias field with
sectional permanent magnets, thereby eliminating the need for the bias
current.

5. Better coating procedures. One of the more troublesome aspects of the
experimental work was maintaining the integrity of the shielding on the
bias coil. The copper used in this coil was not properly treated before
it was coated. Any further work on this project would require more
attention to this aspect of the design.

ACKNOWLEDGMENTS

REFERENCES

1. S.S. Papell, U.S. Patent No. 3,215,572, 1963.

2. S.S. Papell and O.C. Faber, Jr., "On the Influence of Nonuniform Magnetic
    Fields on Ferromagnetic Colloidal Sols," NASA TN D-4676, Lewis Research
    Center, Cleveland, OH, 1968.

3. M.P. Perry, "A Survey of Ferromagnetic Liquid Applications," in
    Thermomechanics of Magnetic Fluids, edited by B. Berkovsky (Hemisphere
    Publishing Co., Washington, DC, 1978) p. 219.

4. B.B. Carey and F.H. Fenlon, "On the Utilization of Ferrofluids for
    Transducer Applications," J. Acoust. Soc. Am., Vol. 45, No. 5, p. 1210,
    1969.

5. J.W. Overby, "A Study of the Feasibility of Development of a Ferrofluid
    Transducer," M.S. Thesis, Florida Institute of Technology, 1978
    (unpublished).

6. P.S. Dubbelday, "Application of ferrofluid as an acoustic transducer
    material," IEEE Transactions on Magnetics, Vol. MAG-16, p. 372, 1980.

7. P.S. Dubbelday and R.W. Timme, U.S. Patent No. 4,361,879, 1980.

8. J.W. Overby, U.S. Patent No. 4,308,602, 1981.

9. P. Pincus, "Static Conformations and Dynamics of Colloidal Suspensions of
    Ferromagnetic Grains," in Thermodynamics of Magnetic Fluids, edited by B.
    Berkovsky (Hemisphere Publishing Co., Washington, DC, 1978) p. 87.

10. C.P. Bean and J.D. Livingston, "Superparamagnetism," J. Appl. Phys., Vol.
    30, 1205-1295, 1959.

11. B. Berkovsky, "Some Aspects of Theoretical Modelling of Thermomechanics of Magnetic Fluids," in Thermomechanics of Magnetic Fluids, edited by B. Berkovsky (Hemisphere Publishing Co., Washington, DC, 1978) p. 149.

12. H. Bogardus, D. Krueger, and D. Thompson, "Dynamic Magnetization in Ferrofluids," in Thermomechanics of Magnetic Fluids, edited by B. Berkovsky (Hemisphere Publishing Co., Washington, DC, 1978) p. 77.

13. R. Kaiser and G. Miskolczy, "Magnetic Properties of Stable Dispersions of Subdomain Magnetic Particles," J. Appl. Phys., Vol. 41, 1064-1072, 1970.

14. V.M. Polunin, "Resonance excitations of oscillations in a ferromagnetic fluid," Magn. Gidrodin, No. 1, p. 141, 1978.

15. V.M. Polunin, "Characteristics of a magnetofluid transducer," Soviet Phys. - Acoustics, Vol. 28, No. 4, p. 318, Jul-Aug 1982.

16. P.S. Dubbelday and M.S. Ptak, "Characteristics of a hydroacoustic ferrofluid projector," J. of Magnetism and Magnetic Materials, Vol. 39, 159-161, 1983).

17. J.L.Neuringer and R.E. Rosensweig, "Ferrohydrodynamics," Phys. Fluids, Vol. 7, p. 1927, 1964.

18. T.D. Jones, "Theory and Application of Ferrofluid Seals," in Thermomechanics of Magnetic Fluids, edited by B. Berkovsky (Hemisphere Publishing Co., Washington, DC, 1978).

19. P. Penfield and H.A. Haus, Electrodynamics of Moving Media, (M.I.T. Press, Cambridge, MA, 1967).

20. P.M. Morse and H. Feshbach, Methods of Theoretical Physics, Part I (McGraw-Hill, New York, 1953) p. 33.

21. M.C. Junger and D. Feit, Sound, Structures, and Their Interaction (M.I.T. Press, Cambridge, MA, 1972) p. 27.

22. M.S. Ptak, "Hydroacoustic Ferrofluid Projector," M.S. Thesis, Florida
    Institute of Technology, 1985 (unpublished).

23. USRD Transducer Catalog, "Underwater Electroacoustic Standard
    Transducers," Naval Research Laboratory, Underwater Sound Reference
    Detachment, Orlando, FL, Apr 1982.

24. P.S. Dubbelday, NRL Memorandum Report 5223, "Measurement of Hydroacoustic
    Particle Motion by Hot-Film Anemometry," Feb 10, 1984.

(blank page)

APPENDIX - PROTOTYPE SPECIFICATIONS

Ferrofluid:

    Type: Lignosite FML
    Manufacturer: Georgia-Pacific Corp.
    Saturation magnetization: $4\pi M$ = 140 G
    Composition: Ferromagnetic Iron Lignosulfonate
    Density: 1.23 gm/cm^3
    Quantity: 3950 cm^3 (1.02 gal)

Ferrofluid Core:

    Radius: 12.07 cm
    Outer radius: 17.15 cm
    Cavity height: 8.26 cm
    Materials: Plexiglas sheet (1/4, 1/3, & 1/16-in. thick)
                Butyl rubber sheet (1/8-in. thick)
                Plexiglas Rod (1/2-in. diam.)
                Seal Screws (1/4-in.)
                4-40 Flat Head Machine Screws
                Epoxy (Resiweld)

Bias Coil:

    Copper plate thickness: 0.11 cm
    Dimensions: see Fig. 6
    Self inductance: 0.49 mH
    Resistance: 23.9 mΩ at 20°C
    Average total length: 88.34 m
    Number of turns: 150
    DC at operating point: 600 A
    Magnetic bias field at operating point: 1230 Oe (9.8×10^4 A/m)
    Power dissipated: 8.63 kW at 20°C
    Material: Copper alloy 110

Insulation: 1) Glyptol Red Enamel (GE #1201)
              2) West System Epoxy 206 Hardener, 105 Resin
                   (Gougeon Bros., Inc.)

Modulation Coil:

Wire size: 19 AWG

Wire type: Heavy-duty magnet wire

Total length: 437.6 m

Number of wires per turn: 8

Number of turns: 150

Resistance: 11.39 Ω at 20°C

Self-inductance: 31 mH

Nominal operating current: 5.4 A

Nominal RMS power dissipation: 332 W at 20°C

Magnetic field amplitude: 126 Oe (10,000 A turns/m)

END

FILMED

2-86

DTIC